

(Supplementary Material)

Pre-operative Assessment of Ablation Margins for Variable Blood Perfusion

Metrics in a Magnetic Resonance Imaging Based Complex Breast Tumour

Anatomy: Simulation Paradigms in Thermal Therapies

Manpreet Singh^{a,c,d,*}, Tulika Singh^b, Sanjeev Soni^c

^aDepartment of Mechanical Engineering, University of Maryland Baltimore County, Baltimore, Maryland, USA; ^bDepartment of Radio-diagnosis and Imaging, Post Graduate Institute of Medical Education and Research, Chandigarh, India; ^cBiomedical Instrumentation Division, CSIR-Central Scientific Instruments Organisation, Chandigarh, India; ^dDepartment of Mechanical Engineering, Thapar Institute of Engineering and Technology University, Patiala, Punjab, India.

***Correspondence to:**

Manpreet Singh, Ph.D (P), M.E.
Department of Mechanical Engineering,
College of Engineering and Information Technology,
University of Maryland Baltimore County,
1000 Hilltop Circle, Baltimore, MD 21250, United States.
Phone: +1-(908) 405-7554; E-mail: snamra.manpreet@gmail.com
Journal: Computer Methods and Programs in Biomedicine
Cover Title: Perfusion Mediated Assessment of Ablation Margins

Supplementary Section-I

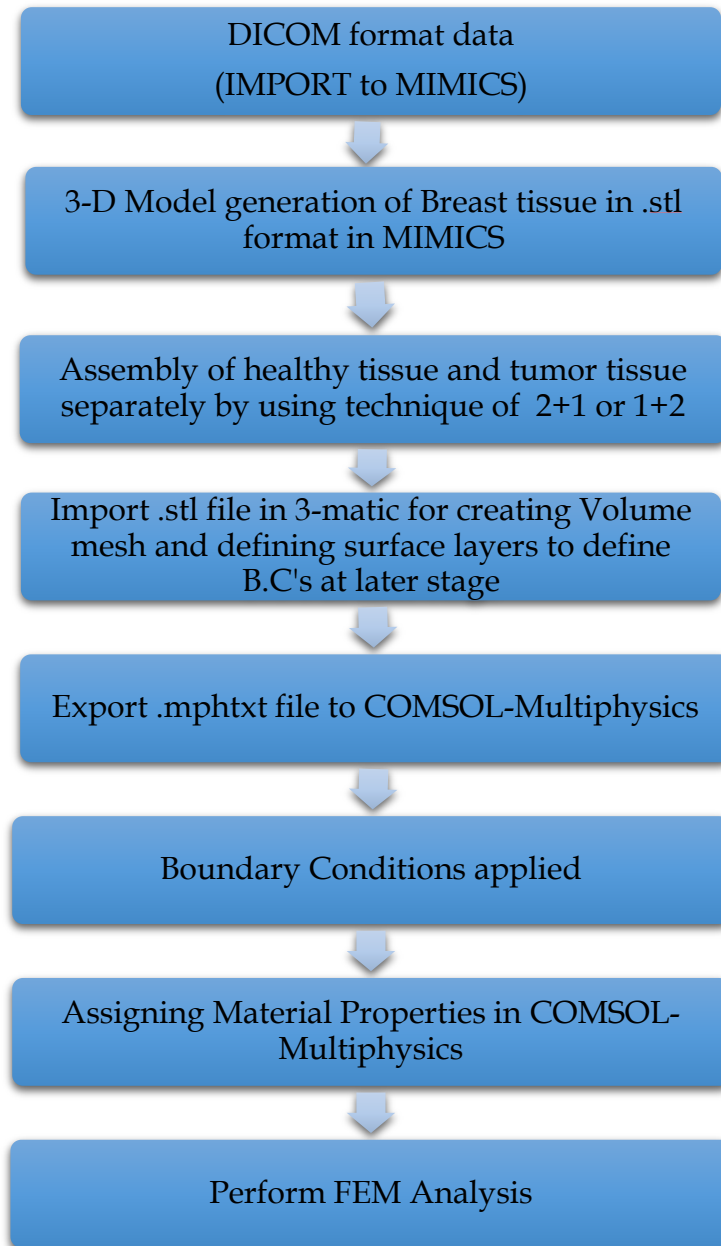


Fig. S1. Flow chart representing the steps performed for the analysis

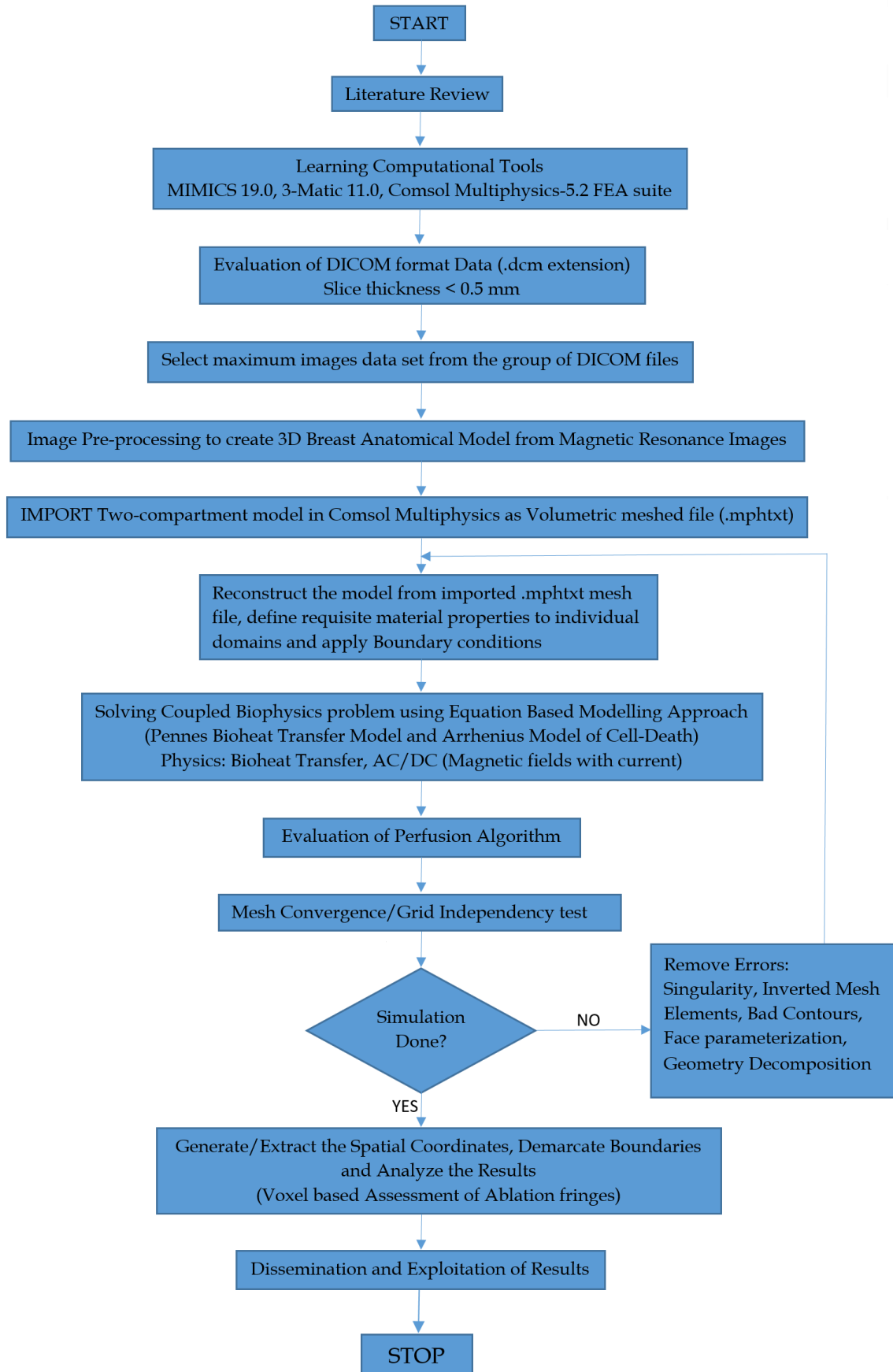


Fig. S2. Flow chart representing the computational approach

Table S1: Mesh Convergence analysis/Grid Independency test

Mesh	Element size	No. of domain elements	No. of boundary elements	No. of edge elements	Max. Volumetric Temp. (in °C)	Variation in results
Mesh 1	Extremely coarse	5,055	2,188	556	90.75	Base
Mesh 2	Extra coarse	7,724	3,020	613	91.88	1.25%
Mesh 3	Coarser	16,271	5,216	819	92.97	1.19%
Mesh 4	Normal	52,379	10,484	955	93.98	1.09%
Mesh 5	Fine	1,33,707	21,802	1,711	94.87	0.95%
Mesh 6	Finer	2,65,505	35,350	2,223	94.89	0.021%
Mesh 7	Extra fine	5,13,507	53,546	2,618	94.90	0.011%

A. Temperature distribution within tumour and healthy tissue interface

Figs. S3 to S6 demonstrates the temperature distribution within tumour and healthy tissue regimes, for various SAR values and exposure durations, in axial/transverse slice view passing through the centre of breast tumour. Tumour region is shown with white background and the temperature contours on the surface are also mapped. Figs. S3a(i), S3b(i), S3c(i), S4a(i), S4b(i), S4c(i), S5a(i), S5b(i), S5c(i), S6a(i), S6b(i), S6c(i) show temperature distribution (Centre slice plots) within breast tumour. Temperature variation within 1-3 mm distance beyond tumour periphery (fringe heating) is shown in Figs. S3a(ii), S3b(ii), S3c(ii), S4a(ii), S4b(ii), S4c(ii), S5a(ii), S5b(ii), S5c(ii), S6a(ii), S6b(ii), S6c(ii) to get detailed information about un-treated/poorly heated nodes of tumour region. This, ‘fringe heating’ in the context of this manuscript is heating of additional healthy tissue layers surrounding tumour i.e. at tumour-healthy tissue interface (Hilger et al., 2001; Hilger et al., 2005a; Tsafnat, 2005). These spatiotemporal temperatures are shown in Fig. S3(c) at 218 seconds, Fig. S4(c) at 170 seconds, Fig. S5(c) at 510 seconds, Fig. S6(c) at 336 seconds respectively for two blood perfusion cases. Multiple iterations were performed and it is found that it is difficult to attain temperature in irregular region of tumour with SAR values less than $1.5 \times 10^6 \text{ Wm}^{-3}$.

The temperature in tumour core is kept below 95°C while to achieve temperature between $45\text{--}55^\circ\text{C}$ at the tumour healthy tissue interfaces. Significant temperature variations can be observed with the progression of exposure duration (time) for variable blood perfusion conditions. It is observed that necrosis zone should be restricted to 3 mm region beyond tumour periphery because further heating leads to thermal damage of healthy breast tissue.

For each SAR value, temperature plots are captured at various time intervals showing propagation of heat from tumour core towards outer boundaries of tumour (shown with white arrows). Yellow and blue dotted lines marked in Figs. S3a(ii), S3b(ii) and S3c(ii) show 1 mm and 3 mm zones (beyond tumour boundary). The temperature achieved in 1 mm zone, as shown in Fig. S3c(ii), is in the range of $60\text{--}65^\circ\text{C}$ (thermal ablation).

A.1. Homogeneously perfused tumour tissue, variable moderate blood perfusion

$$\text{Fat tissue-}\omega_b = 8.3 \times 10^{-3} [\text{s}^{-1}], \text{ Tumour tissue-}\omega_b = 5 \times 10^{-4} [\text{s}^{-1}]$$

Based on the simulation runs, two SAR values i.e. $1.6 \times 10^6 \text{ Wm}^{-3}$ and $1.8 \times 10^6 \text{ Wm}^{-3}$ are chosen for moderately perfused tumour and corresponding results are shown in Fig. S3 and Fig.S4. Fig. S3 illustrates temperature distribution for SAR of $1.6 \times 10^6 \text{ Wm}^{-3}$ for duration of 218 seconds at three time intervals. Fig. S4 shows temperature distribution for SAR of $1.8 \times 10^6 \text{ Wm}^{-3}$ for duration of 170 seconds at three time intervals.

Temperature within tumour core was restricted below 95°C to avoid tissue carbonisation. It can be seen from Fig. S3 that for SAR value of $1.6 \times 10^6 \text{ Wm}^{-3}$ at 218 seconds, entire tumour core attains temperatures higher than 85°C whereas the tumour periphery attains an average temperature of 50°C . Outside of 1-3 mm zone beyond tumour periphery, the temperature is within safe limits of 37°C . Further increasing SAR value to $1.8 \times 10^6 \text{ Wm}^{-3}$ for 170 seconds, the temperature within tumour core becomes $\sim 90^\circ\text{C}$ while tumour periphery reaches 52°C . For duration of 218 seconds, the temperature of tumour irregular region, as seen from Figs. S3a(i), S3a(ii), S3a(iii), is $\sim 45^\circ\text{C}$ which is sufficient for hyperthermia. The temperature within 1 mm distance beyond tumour boundary is higher than 60°C and for 3 mm zone it is higher than 45°C . In Fig. S3, the red dotted lines show poorly heated tumour region but this is very less.

Blood perfusion at the tumour-healthy tissue interface increases with increase in temperature, thereby restricts the temperatures attained in this region through heat sink effect. So, there is requirement of additional heat delivery to balance/overcome the heat loss which can be achieved through higher SAR and exposure duration.

Exposure durations with higher SAR values are also compared for moderately perfused tumour (Fig. S3 vs. Fig. S4) and highly perfused tumour (Fig. S5 vs. Fig. S6). It can be seen from Fig. S3 and S4 that, for moderate blood perfusion, by increasing SAR value from $1.6 \times 10^6 \text{ Wm}^{-3}$ to $1.8 \times 10^6 \text{ Wm}^{-3}$, the exposure time reduces by 48 seconds. This reduction may be useful for patients having poor heat tolerable capacity. It is demonstrated in Fig. S5 and Fig. S6 that, for highly perfused tumour, with SAR values of $2.0 \times 10^6 \text{ Wm}^{-3}$ to $2.2 \times 10^6 \text{ Wm}^{-3}$, the heating zone propagates from tumour core towards irregular region (extremities of tumour) in shorter duration and with more tumour coverage. The exposure time in this case is reduced by 34% i.e. it takes 174 seconds less. Further, highly perfused tissue takes longer time for attaining thermal ablation temperatures as compared to moderately perfused tumour.

A.2. Homogeneously perfused tumour tissue, variable high blood perfusion

$$\text{Fat tissue-}\omega_b = 1 \times 10^{-2}[\text{s}^{-1}]; \text{ Tumour tissue-}\omega_b = 5.3 \times 10^{-2}[\text{s}^{-1}]$$

Here, iterative simulations were conducted for highly perfused tumour and two SAR values were chosen as $2.0 \times 10^6 \text{ Wm}^{-3}$ and $2.2 \times 10^6 \text{ Wm}^{-3}$ and corresponding results are presented. Temperature distributions for these SAR values are shown in Fig. S5 for duration of 510 seconds at three time intervals and in Fig. S6 for duration of 336 seconds with three time intervals. Results show that higher exposure duration (magnetic field ON) is required for high blood perfusion values as compared with moderate blood perfusion. Poorly heated regions within tumour extremities are reduced with

proportional increase in SAR value to $2.2 \times 10^6 \text{ Wm}^{-3}$. It can be clearly seen that exposure duration is considerably reduced by 174 seconds as compared to the perfusion conditions discussed in first case.

It is illustrated in Fig. S5 that with SAR value of $2.0 \times 10^6 \text{ Wm}^{-3}$ for 510 seconds, entire tumour core attains temperatures of $\sim 90^\circ\text{C}$ whereas the tumour periphery attains an average temperature of 45°C . As followed from Fig. S5c(ii), temperature isotherm corresponding to 60°C is attained all around the tumour (within 0.5 mm distance from tumour periphery) and in some regions this condition is satisfied up to 1 mm distance. In additional 2-3 mm heated region, the temperatures are between 45°C and 55°C . Beyond 3 mm zone, the temperature is 37°C - 40°C which is within safe limit. It can be seen from Fig. S6a(i) and Fig. S6a(ii) that for duration of 84 seconds, the temperature at tumour core is 45°C and the temperature at irregular region of tumour is less than 41°C . On increasing the exposure duration to 168 seconds, as shown in Fig. S6b(i) and Fig. S6b(ii), the temperature at tumour core becomes 48°C while the temperature at irregular tumour region is still less than 41°C which means exposure duration needs to be further increased. It can be seen from Figs. S6a(i), S6b(i), S6c(i) that for increased SAR value of $2.2 \times 10^6 \text{ Wm}^{-3}$ at 336 seconds, the core tumour temperatures is $\sim 90^\circ\text{C}$ and tumour periphery is at an average of 49°C . The temperature achieved in tumour irregular region (at periphery) is $\sim 42^\circ\text{C}$ which is in mild hyperthermia range. The temperature within 1 mm distance beyond tumour periphery (tumour-tissue interface zone) is higher than 55°C and within 3 mm zone it is 45 - 53°C . In Fig. S6, red marked dotted lines (for tumour irregular nodes) show poorly heated zone, which is minimal.

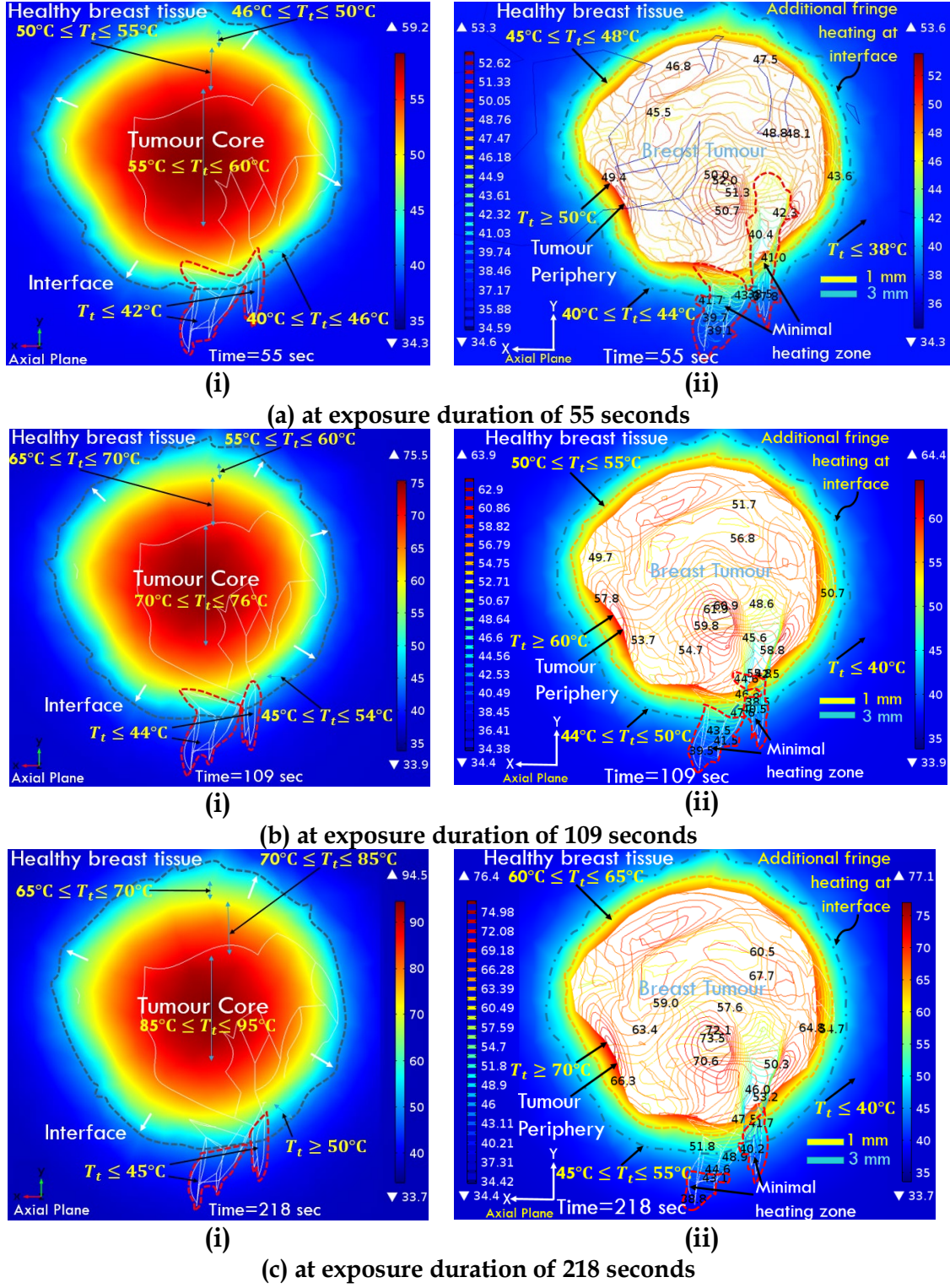


Fig. S3. Temperature distribution within tumour and healthy breast, considering Specific Absorption Rate (SAR) as $1.6 \times 10^6 \text{ Wm}^{-3}$ at three time intervals. Surface temperature contours are shown in R.H.S (a(ii), b(ii), c(ii)) while center slice plots at tumour core are shown in L.H.S (a(i), b(i), c(i)). Tumour region is shown with white background color. Temperature variation is texted in 1-3 mm region adjacent to the tumour periphery. Heating zone propagates from tumour core towards irregular nodes of tumour. **Moderately perfused** tissue is considered with fat tissue perfusion as $8.3 \times 10^{-3} [\text{s}^{-1}]$ and tumour perfusion as $5 \times 10^{-4} [\text{s}^{-1}]$. Yellow dotted line represents 1 mm heated region while blue dotted line represents 3 mm heated region. Red dotted line show poorly heated tumour region.

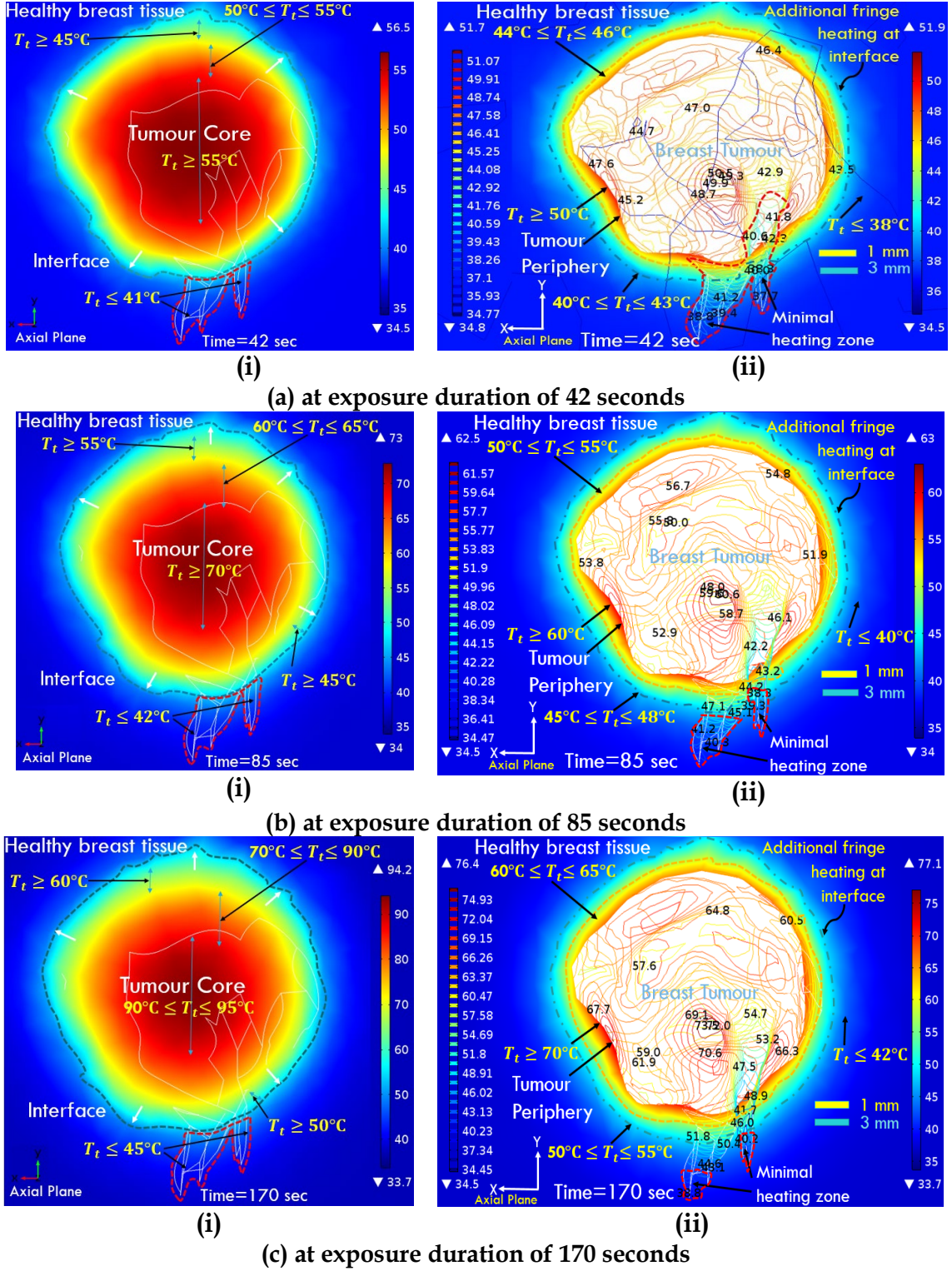


Fig. S4. Temperature distribution within tumour and healthy breast, considering Specific Absorption Rate (SAR) as $1.8 \times 10^6 \text{ Wm}^{-3}$ at three time intervals. Surface temperature contours are shown in R.H.S (a(ii), b(ii), c(ii)) while center slice plots at tumour core are shown in L.H.S (a(i), b(i), c(i)). Tumour region is shown with white background color. Temperature variation is texted in 1-3 mm region adjacent to the tumour periphery. Heating zone propagates from tumour core towards irregular nodes of tumour. **Moderately perfused** tissue is considered with fat tissue perfusion as $8.3 \times 10^{-3} [\text{s}^{-1}]$ and tumour perfusion as $5 \times 10^{-4} [\text{s}^{-1}]$. Yellow dotted line represents 1 mm heated region while blue dotted line represents 3 mm heated region. Red dotted line show poorly heated tumour region.

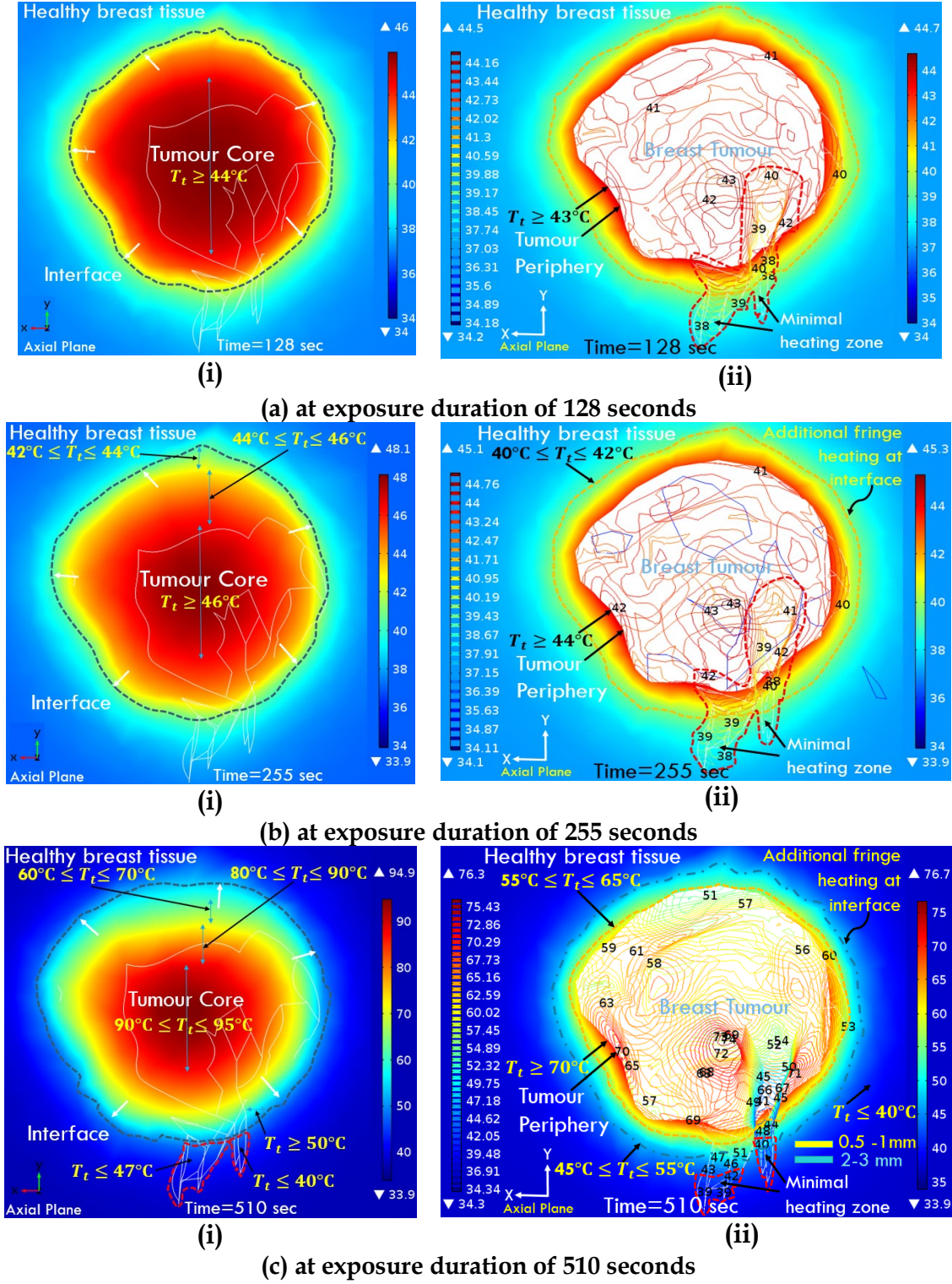


Fig. S5. Temperature distribution within tumour and healthy breast, considering Specific Absorption Rate (SAR) as $2 \times 10^6 \text{ Wm}^{-3}$ at three time intervals. Surface temperature contours are shown in R.H.S (a(ii), b(ii), c(ii)) while center slice plots at tumour core are shown in L.H.S (a(i), b(i), c(i)). Tumour region is shown with white background color. Temperature variation is texted in 1-3 mm region adjacent to the tumour periphery. Heating zone propagates from tumour core towards irregular nodes of tumour. **Highly perfused** tissue is considered with fat tissue perfusion as $1.0 \times 10^{-2} [\text{s}^{-1}]$ and tumour perfusion as $5.3 \times 10^{-2} [\text{s}^{-1}]$. Yellow dotted line represents 1 mm heated region while blue dotted line represents 3 mm heated region. Red dotted line show poorly heated tumour region.

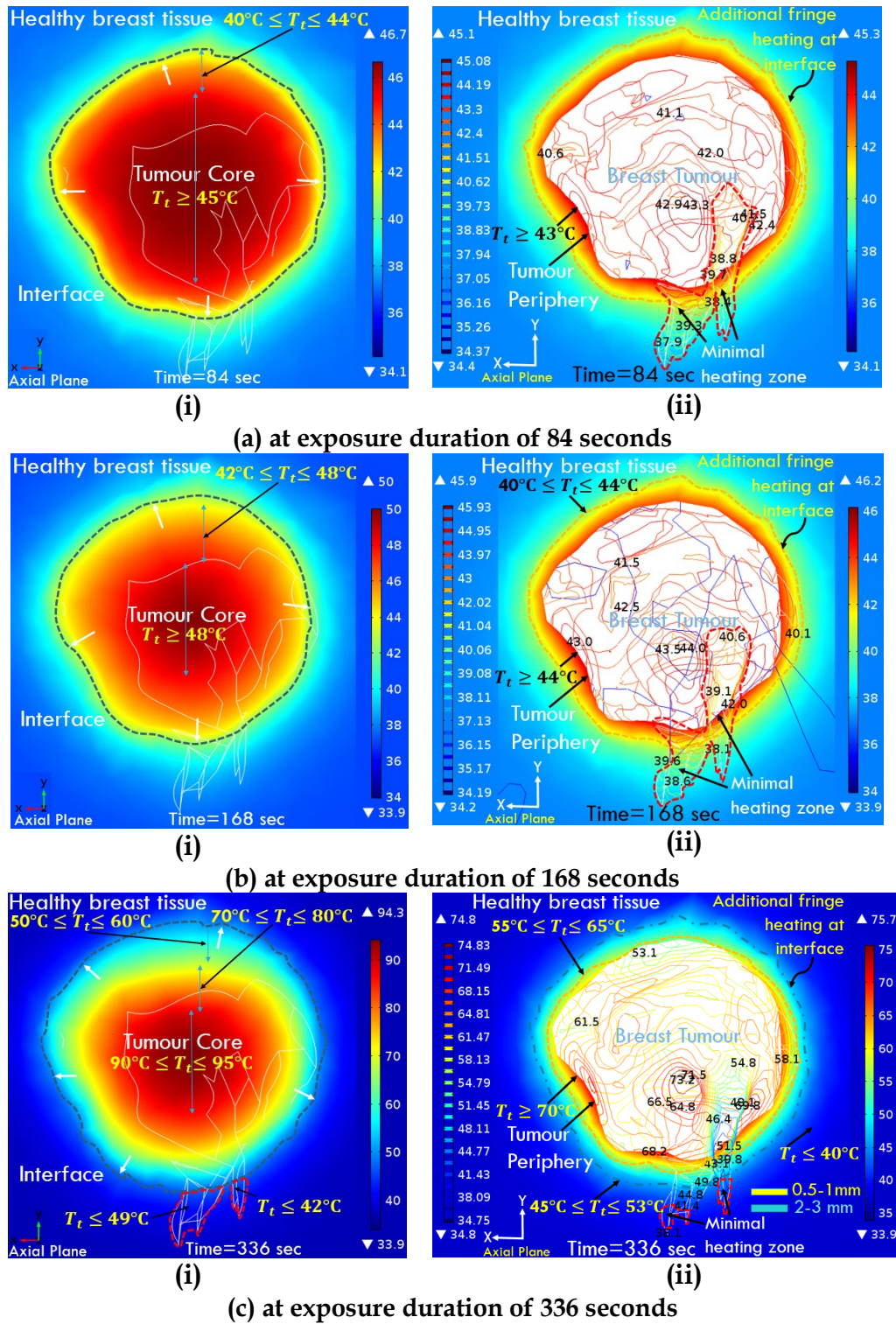


Fig. S6. Temperature distribution within tumour and healthy breast, considering Specific Absorption Rate (SAR) as $2.2 \times 10^6 \text{ Wm}^{-3}$ at three time intervals. Surface temperature contours are shown in R.H.S (a(ii), b(ii), c(ii)) while center slice plots at tumour core are shown in L.H.S (a(i), b(i), c(i)). Tumour region is shown with white background color. Temperature variation is texted in 1-3 mm region adjacent to the tumour periphery. Heating zone propagates from tumour core towards irregular nodes of tumour. **Highly perfused** tissue is considered with fat tissue perfusion as $1.0 \times 10^{-2} [\text{s}^{-1}]$ and tumour perfusion as $5.3 \times 10^{-2} [\text{s}^{-1}]$. Yellow dotted line represents 1 mm heated region while blue dotted line represents 3 mm heated region. Red dotted line show poorly heated tumour region.

B. Thermal damage at tumour and tumour-healthy tissue interface

This section discusses thermal damage within tumour and at tumour-tissue interface, evaluated for different SAR and exposure duration pertaining to tumour blood perfusion conditions. Thermal damage is also compared with corresponding temperature contours at different time intervals to analyse the effect of localised heating.

B.1. Homogeneously perfused tumour tissue, variable moderate blood perfusion

$$\text{Fat tissue-}\omega_b = 8.3 \times 10^{-3} [s^{-1}]; \text{ Tumour tissue-}\omega_b = 5 \times 10^{-4} [s^{-1}]$$

Fig. S7 and Fig. S8 show thermal damage within tumour (in Axial/Transverse slice passing through the centre of breast tumour) and at tumour-tissue interface considering SAR values of $1.6 \times 10^6 \text{ Wm}^{-3}$ and $1.8 \times 10^6 \text{ Wm}^{-3}$ for different exposure durations. Estimation of thermal damage within 1–3 mm distance beyond tumour boundaries is also done.

It can be seen from Fig. S7 that for a moderately perfused tumour with SAR value of $1.6 \times 10^6 \text{ Wm}^{-3}$, the thermal damage propagates from tumour core towards irregular region of tumour. At duration of 55 seconds, the thermal damage parameter (Ω) at center of tumour is ~ 10 while at tumour boundary, there is almost zero damage. It can be seen from Figs. S3b(ii) and S7b(ii) that with increase in duration to 109 seconds, poorly heated zone (shown with red dotted line) is significantly reduced. From Fig. S7b(ii), it can be seen that there are irregular depressions over the surface of tumour corresponding to thermal damage, $\Omega < 2$. From Fig. S7b(ii), it is noted that entire tumour core attains $\Omega=10$ within 109 seconds but the thermal damage (Ω) is less than one on the tumour surface. The fringes (tissue layers) corresponding to 0.5 mm distance (beyond tumour boundary) show Ω values as 6-7 while at 1 mm distance from tumour boundary, Ω is 3-4. Within irregular tumour region Ω is 0-2, which corresponds to temperature less than 45°C from (as shown in Fig. S3b(ii)). On increasing the duration from 109 seconds to 218 seconds, temperature within the tumour core becomes $85\text{-}95^\circ\text{C}$ and the temperature at 1 mm distance from tumour boundary (shown as yellow dotted line) is $60\text{-}65^\circ\text{C}$. The temperature at surface of tumour is $\sim 70^\circ\text{C}$. Here 3 mm region shows Ω as 3-4.5 and beyond 3 mm distance, there is almost nil damage to healthy breast tissue.

For moderately perfused tumour, on further increasing the SAR value to $1.8 \times 10^6 \text{ Wm}^{-3}$ the thermal damage is shown in Fig. S8. At duration of 42 seconds, the temperature at centre of tumour core is 55°C and thermal damage is 10 in a confined area (shown in Fig. S8a(i)) while the temperature at tumour periphery is 45°C which shows that thermal damage is not yet attained at the surface of tumour and beyond tumour boundaries. Temperature at the irregular region is $< 42^\circ\text{C}$ as shown by red dotted lines.

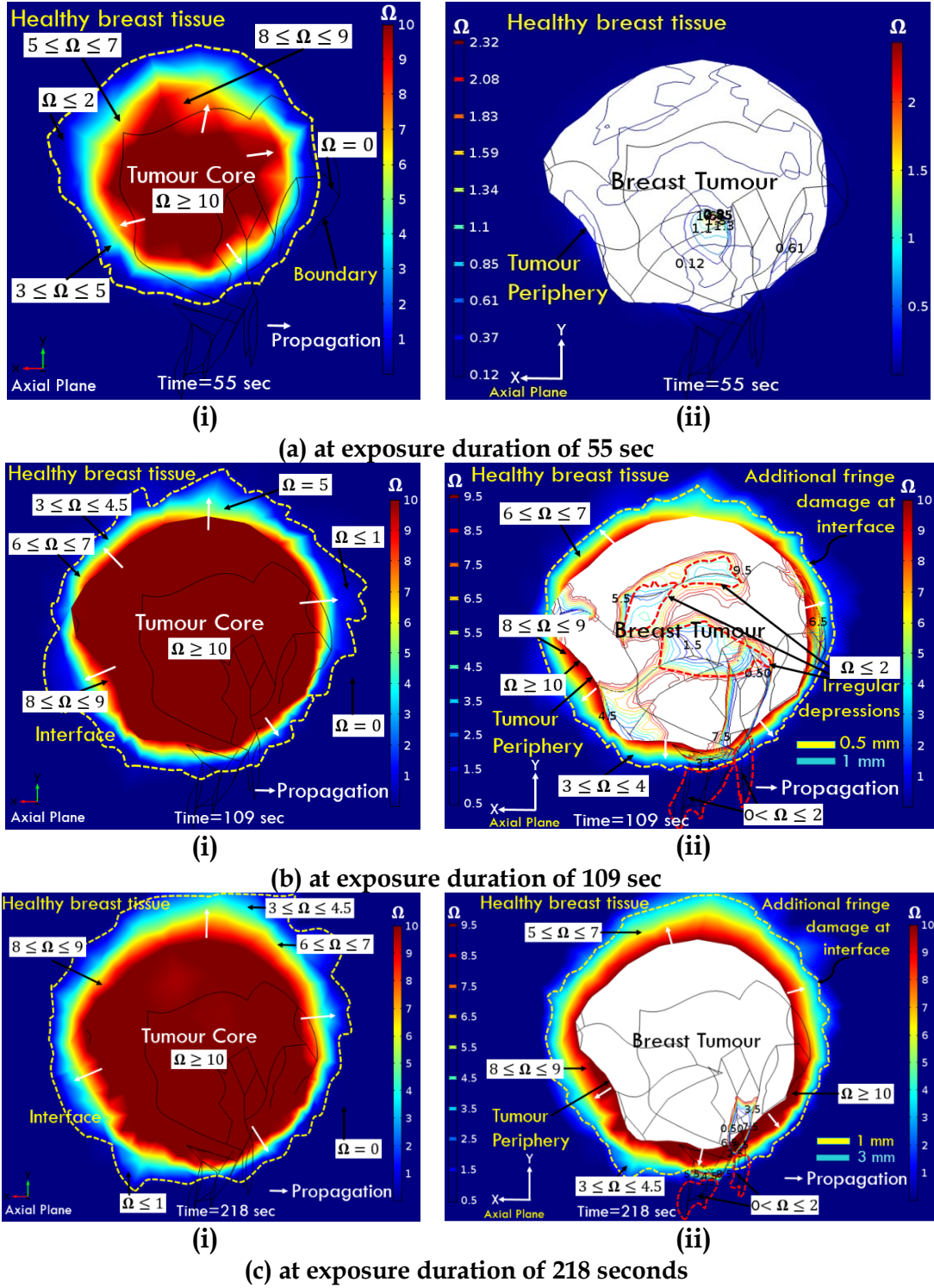


Fig. S7. Thermal damage within tumour and healthy tissue considering Specific Absorption Rate (SAR) value as $1.6 \times 10^6 \text{ Wm}^{-3}$ at different time intervals. Thermal damage contours are shown in R.H.S (a(ii), b(ii), c(ii)) while center slice plots at tumour core are shown in L.H.S (a(i), b(i), c(i)). Thermal damage front is shown in 1-3 mm region adjacent to the tumour periphery. Tumour volume is shown with white background. **Moderately perfused** tissue is considered with perfusion of fat tissue as $8.3 \times 10^{-3} [\text{s}^{-1}]$ and tumour tissue as $\omega_b = 5 \times 10^{-4} [\text{s}^{-1}]$.

On increasing the exposure duration to 85 seconds, the thermal damage front covers almost whole of the tumour parenchyma. Thermal damage, Ω at tumour-tissue interface is 3.5-4.5 as shown in Fig. S8b(i) which corresponds to temperature of 60-65°C as seen from Fig. 4b(i). It can also be observed from Fig. S8b(ii), that some fringes within 5 mm distance (from tumour boundary) attain $\Omega < 1$ while tissue layers at periphery attain Ω as 6-7. This non-uniform thermal damage is attributed to the irregular shape of tumour which occurs in real practice and is a clinical challenge to ablate. As the protocol considered in this study is to confine the thermal damage (Ω of 4-10) within 3 mm region beyond tumour to have effective treatment, the exposure duration is doubled from 85 seconds to 170 seconds to ensure thermal damage of tumour especially at tumour irregular region.

As per Fig. S8c(i), at the exposure time of 170 seconds, the thermal damage within tumour core is 10 while at 1 mm fringe distance it is 6-7 as shown in Fig. S8c (ii). Fringes at 3 mm distance attain Ω as 3 - 4.5. Still, there is a marginal portion on irregular region of tumour with $\Omega < 4$ which is still acceptable to stop the heating. It was observed that further heating will damage the healthy breast tissue beyond 5 mm distance, which is not acceptable because the induced damage exceeds 1.5 times the tumour volume. This SAR value is in agreement with recent experimental heat dosage value reported for magnetic nanoparticle hyperthermia (Gu et. al., 2019).

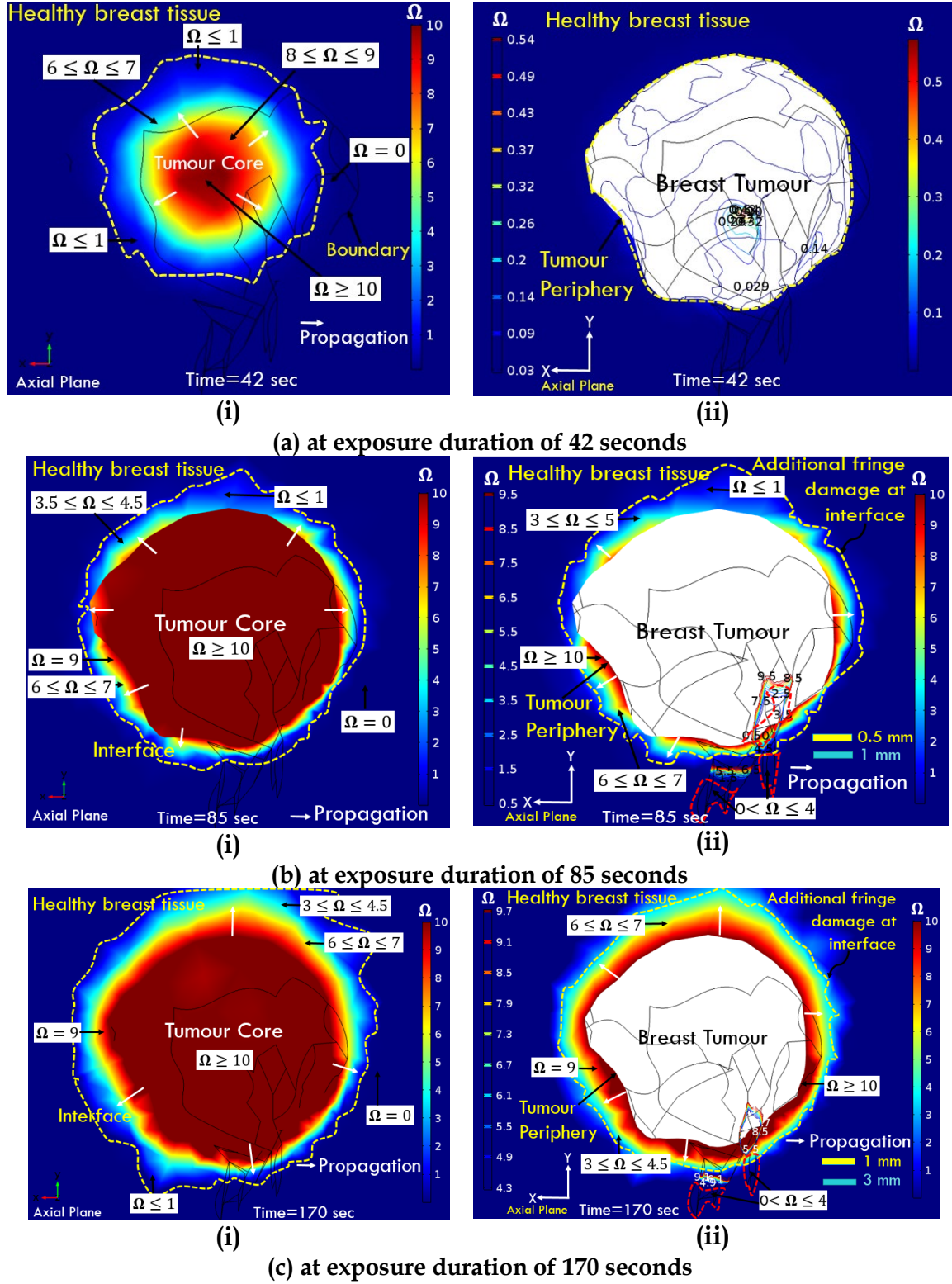


Fig. S8. Thermal damage within tumour and healthy tissue considering Specific Absorption Rate (SAR) value as $1.8 \times 10^6 \text{ Wm}^{-3}$ at different time intervals. Thermal damage contours are shown in R.H.S (a(ii), b(ii), c(ii)) while center slice plots at tumour core are shown in L.H.S (a(i), b(i), c(i)). Thermal damage front is shown in 1-3 mm region adjacent to the tumour periphery. Tumour volume is shown with white background. **Moderately perfused** tissue is considered with perfusion of fat tissue as $8.3 \times 10^{-3} [\text{s}^{-1}]$ and tumour tissue as $\omega_b = 5 \times 10^{-4} [\text{s}^{-1}]$.

B.2. Homogeneously perfused tumour tissue, variable high blood perfusion

$$\text{Fat tissue-}\omega_b = 1 \times 10^{-2} [s^{-1}]; \text{ Tumour tissue-}\omega_b = 5.3 \times 10^{-2} [s^{-1}]$$

Figs. S9 and S10 demonstrates thermal damage for highly perfused tumour considering SAR values of $2.0 \times 10^6 \text{ Wm}^{-3}$ and $2.2 \times 10^6 \text{ Wm}^{-3}$ respectively. Figs. S9a (i) and S9a(ii), demonstrates that for a highly perfused tumour tissue (SAR $2.0 \times 10^6 \text{ Wm}^{-3}$), the thermal damage is minimal (no damage) at 128 seconds with corresponding average temperature of 44°C (refer Fig. S5a(i) and Fig. S5a(ii)) in tumour core and is less than 40°C at tumour irregular region. So, exposure duration was doubled to 255 seconds to achieve desired thermal damage within tumour especially in irregular region of tumour within bound of 5 mm (Singh and Repaka, 2017b). For this duration of 255 seconds, it was found that thermal damage was less than one at tumour core with corresponding temperature increase of just 2°C and while the temperature at irregular region of tumour is less than 41°C . This insignificant heat response of breast tumour is due to high blood perfusion of tumour. So there is need to either increase the exposure duration or increase the SAR value. Both the cases were considered and the evaluated results are shown in Fig. S6 and Fig. S10. Corresponding results for increased duration of 510 seconds are shown in Fig. S5c(i) and S5c(ii). It is seen from Fig. S5c(i) and S5c(ii) that the temperature in tumour core is $\sim 95^\circ\text{C}$ and it is 47°C at irregular region of tumour which is within hyperthermic range. In Fig. S5c(ii) i.e. surface temperature contours of breast tissue show temperature variation as $50\text{--}60^\circ\text{C}$. For same parameters, it is seen from Fig. S9c(i) and Fig. S9c(ii) that thermal damage within tumour is 10. Fringe heating in 1-2 mm distance (beyond tumour boundary) shows thermal damage (Ω) as 5-7 whereas at 3 mm distance Ω is 3-5. It is observed that thermal damage slightly extends outside the 3 mm distance (beyond tumour boundary) as shown in Fig. S9c(ii) but still it is within bound of 5 mm healthy breast region which is acceptable as per literature. Most of the tumour irregular region attained thermal damage of 2 which seems reasonable.

The next possibility to reduce the exposure duration is by increasing SAR value to $2.2 \times 10^6 \text{ Wm}^{-3}$ is also investigated and the corresponding thermal damage results are shown in Fig. S10. It is very interesting to see that for exposure duration of 168 seconds, the thermal damage remains less than 1 for highly perfused tumour even at corresponding temperature of 48°C . Therefore, exposure duration is doubled to 336 seconds, and the results are shown in Fig. S10c(i) and S10c(ii). It is seen that required Ω value of 10 is achieved within tumour core, Ω of 8 is achieved on tumour boundary and Ω of 6-7 is attained within fringes at 1-2 mm distance from tumour boundaries. While Ω of 3-5 is attained at 3 mm region beyond tumour boundary, which is acceptable. It can be seen from Fig. S10c(ii) that major portion of irregular region of tumour is damaged (Ω of 9-10) with insignificant region having Ω value of 2. Corresponding temperature within irregular tumour region is 49°C while at 2-3 mm distance the temperature is $45\text{--}53^\circ\text{C}$. Also, beyond the heated fringes, the healthy tissue remains at normal body temperature of 37°C . The iterative computational experiments suggest margins less than 5 mm are sufficient enough for the given patient-specific tumour rather than sacrificing typical 10 mm excessive healthy tissue fringes criterion used clinically.

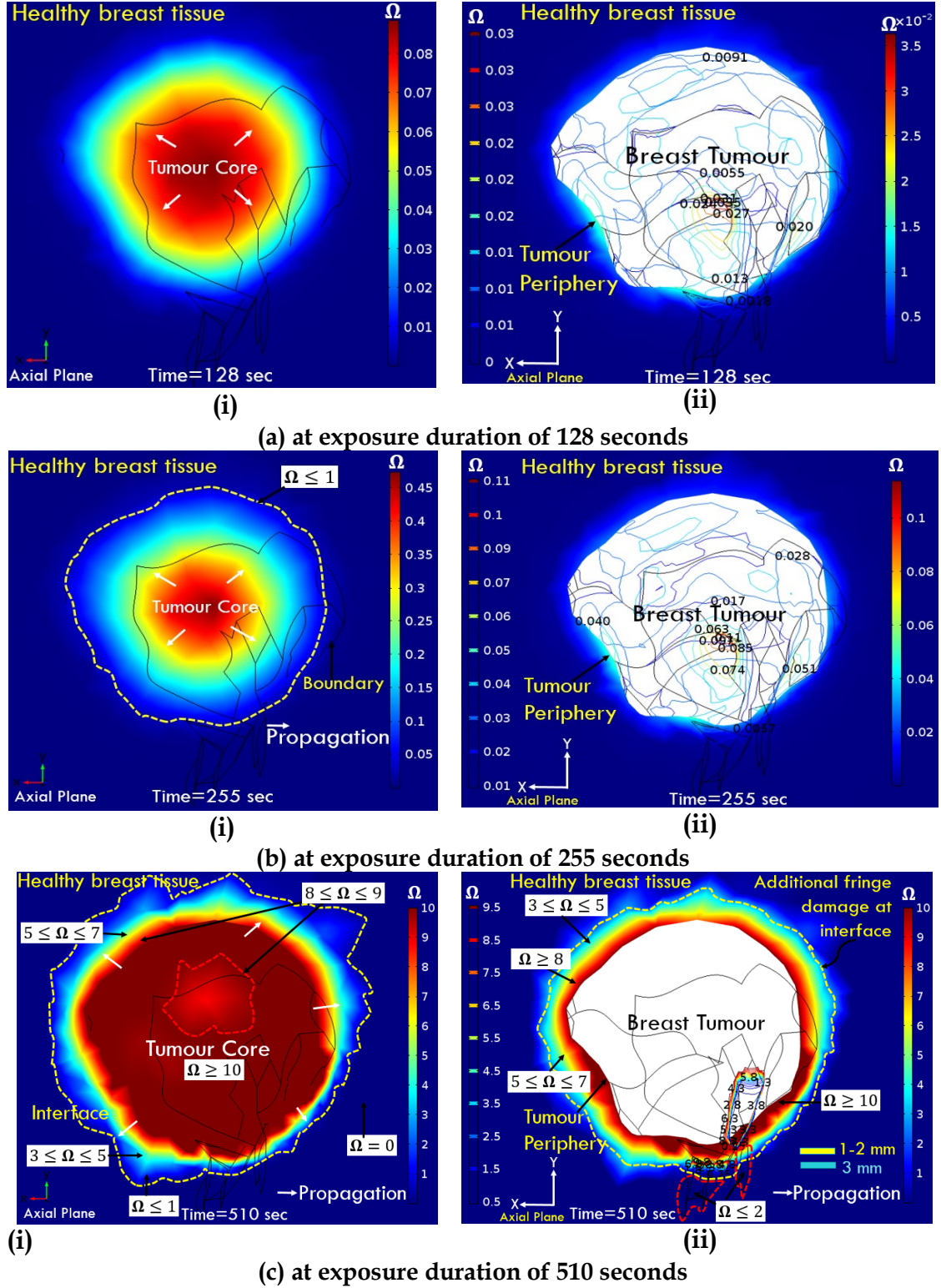


Fig. S9. Thermal damage within tumour and healthy tissue considering Specific Absorption Rate (SAR) value as $2 \times 10^6 \text{ Wm}^{-3}$ at different time intervals. Thermal damage contours are shown in R.H.S (a(ii), b(ii), c(ii)) while center slice plots at tumour core are shown in L.H.S (a(i), b(i), c(i)). Thermal damage front is shown in 1-3 mm region adjacent to the tumour periphery. Tumour volume is shown with white background. **Highly perfused** tissue is considered with perfusion of fat tissue as $1.0 \times 10^{-2} [\text{s}^{-1}]$ and tumour tissue as $\omega_b = 5.3 \times 10^{-2} [\text{s}^{-1}]$.

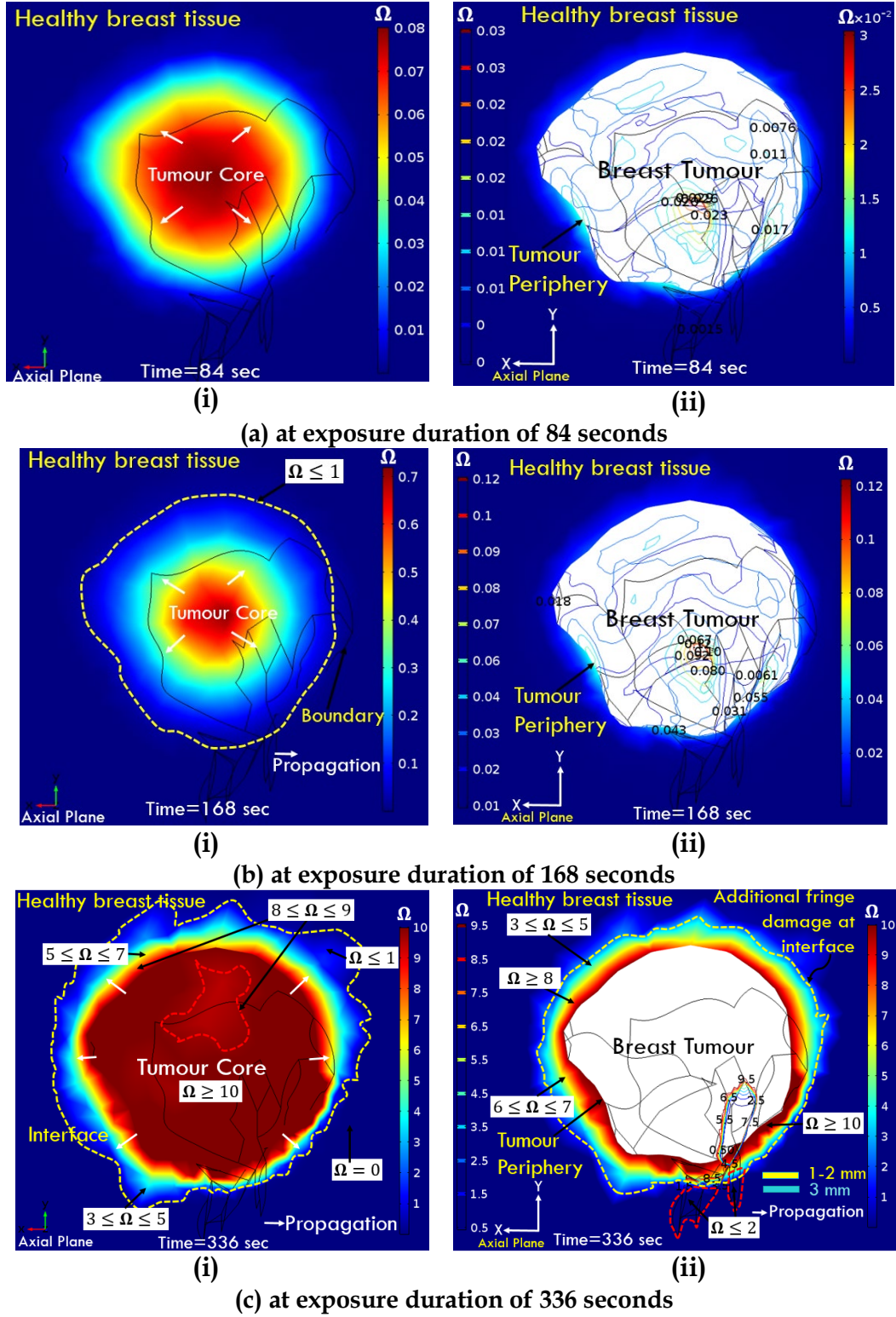


Fig. S10. Thermal damage within tumour and healthy tissue considering Specific Absorption Rate (SAR) as $2.2 \times 10^6 \text{ Wm}^{-3}$ at different time intervals. Thermal damage contours are shown in R.H.S (a(ii), b(ii), c(ii)) while center slice plots at tumour core are shown in L.H.S (a(i), b(i), c(i)). Thermal damage front is shown in 1-3 mm region adjacent to the tumour periphery. Tumour volume is shown with white background. **Highly perfused** tissue is considered with perfusion of fat tissue as $1.0 \times 10^{-2} [\text{s}^{-1}]$ and tumour tissue as $\omega_b = 5.3 \times 10^{-2} [\text{s}^{-1}]$.

Supplementary Section-II

Parametric Formulation for Power dissipation for Superparamagnetic Nanoparticle Heating

From the first law of thermodynamics,

$$\delta Q = \delta U + \delta W \quad (9)$$

where, U is the internal energy, Q is the heat added, W is the magnetic work done on the system (taken as negative);

$$\begin{aligned} \delta Q &= \delta U + (-\delta W) \\ \therefore, \delta Q &= \delta U - \delta W \end{aligned} \quad (10)$$

Since, for an adiabatic process, $\delta Q = 0$;

$$\Rightarrow \delta U = \delta W \quad (11)$$

Differential magnetic work can be written as $\delta W = H \cdot dB$

$$\Rightarrow \delta U = H \cdot dB \quad (12)$$

$$\text{where, } B = \mu_o (H + M) \quad (13)$$

where, H is the magnetic field intensity, B is the induction, μ_o is the permeability of free space, M is the material magnetization, which is a function of applied field and magnetic susceptibility,

$$\delta U = -\mu_o \oint M dH \quad (14)$$

When magnetization lags the field, integration yields positive results indicating conversion of magnetic work into internal energy. Expressing magnetization in terms of complex ferrofluid susceptibility,

$$\chi = \chi' + \chi'' \quad (15)$$

χ' is the in-phase component of χ and χ'' is the out of phase component of χ (term relates to material parameters of ferrofluid) called loss component

$$H(t) = H_o \cos \omega t = \text{Re}[H_o e^{i\omega t}] \quad (16)$$

we know; $e^{i\omega t} = \cos \omega t + i \sin \omega t$

= Real part + Imaginary part

$$M(t) = \text{Re}[\chi H_o e^{i\omega t}] = H_o [\chi' \cos \omega t + \chi'' \sin \omega t] \quad (17)$$

$$\delta U = 2\mu_o H_o^2 \chi'' \int_0^{2\pi/\omega} \sin^2 \omega t \quad (18)$$

we know; $\omega = 2\pi f$

$$\Rightarrow f = \frac{\omega}{2\pi}$$

$$\text{Volumetric power dissipation, } P = f \cdot \delta U = \pi \mu_o f H_o^2 \chi'' \quad (19)$$

Writing equation for motionless fluid in oscillatory field as;

$$\frac{\partial M(t)}{\partial t} = \frac{1}{\tau_R} (M_o(t) - M(t)) \quad (20)$$

$$\text{Equilibrium Magnetization, } M_o(t) = \chi_o H_o \cos \omega t = \text{Re}[\chi_o H_o e^{i\omega t}] \quad (21)$$

Complex Susceptibility in terms of equilibrium susceptibility, $\chi = \frac{\chi_o}{1 + i\omega \tau_R}$

Complex Susceptibility depends upon frequency and effective relaxation time,

$$\chi' = \frac{\chi_o}{1+(\omega\tau_R)^2} = \frac{\chi_o}{1+(2\pi f\tau_R)^2} \quad (22)$$

$$\chi'' = \frac{\omega\tau_R}{1+(\omega\tau_R)^2} \chi_o = \frac{2\pi f\tau_R}{1+(2\pi f\tau_R)^2} \chi_o \quad (23)$$

Reinvoking, Volumetric power dissipation,

$$\begin{aligned} P &= \pi\mu_o f H_o^2 \chi'' \\ &= \pi\mu_o f H_o^2 \left(\frac{2\pi f\tau_R}{1+(2\pi f\tau_R)^2} \chi_o \right) \\ &= \pi\mu_o \chi_o H_o^2 f \left(\frac{2\pi f\tau_R}{1+(2\pi f\tau_R)^2} \right) \end{aligned} \quad (24)$$

This expression is equivalent to SAR in watts per cubic meter of fluid (or tissue) i.e. (SAR=P). This can be easily converted into more standard units of cubic centimeters or gram tissue. In addition, absorption for magnetic nanoparticles is often expressed in terms of watts per mass iron, which is obtained by dividing the expression by the product of bulk density of iron in the nanoparticles (ρ_{Fe}) and the nanoparticle volume fraction (ϕ). The SAR can also be expressed as in terms of Specific Loss Power (S.L.P) in units of $W/g_{magnetite}$. Ultimately, patient-specific medical image based approach is shown to relate temperature-history to cell-death could be used to predict the therapeutic region in realistic time during the heating process, thereby allowing one to treat the irregular tumour boundaries and sparing margins of adjoining critical tissues.

$$S.L.P_{magnetite} = \frac{SAR_{spm}}{\phi\rho_{magnetite}} \quad (25)$$

SAR evaluation

Given the extrinsic (i.e. shape, diameter) and intrinsic (i.e. magnetization) properties of the particles and the intensity value of the exciting magnetic field, a specific MATLAB (Mathworks, Natick, MA) code procedure was developed to obtain an estimate of the effective power density (W/m^3) originating from the considered magnetizing fluid. For a monodisperse solution, this power is given by,

$$SAR_{spm} = \pi\mu_o \chi_o H_o^2 f \left(\frac{2\pi f\tau_R}{1+(2\pi f\tau_R)^2} \right) \quad (26)$$

where, μ_o is the permeability of free space $= 4\pi \times 10^{-7} Tm/A$, χ_o is the equilibrium susceptibility, H_o is the AMF (Alternating Magnetic Field) strength, f is the AMF frequency, τ_R is the effective relaxation time. The effective relaxation time is given as

$$\frac{1}{\tau_R} = \frac{1}{\tau_N} + \frac{1}{\tau_B} \text{ or } \tau_R = \frac{(\tau_N \cdot \tau_B)}{\tau_N + \tau_B} \quad (27)$$

wherein Eqn. (27) the symbols, τ_N and τ_B are the Neel relaxation and Brownian relaxation time, respectively. The relationship between τ_N and τ_B are expressed as:

$$\tau_N = \frac{\sqrt{\pi}}{2} \tau_o \frac{\exp\left(\frac{KV_M}{k_B T}\right)}{\sqrt{\frac{KV_M}{k_B T}}} \text{ and } \tau_B = \frac{3\eta V_H}{k_B T} \quad (28)$$

wherein Eqn. (28) the symbols, τ_o is the average relaxation time in response to a thermal fluctuation is 10^{-9} sec or 10^{-11} sec, η is the viscosity of fluid/medium, k_B is the Boltzmann's constant $1.38 \times 10^{-23} \text{ J/K}$, T is the temperature, K being the anisotropy constant of MNP, V_H is the hydrodynamic volume of MNPs that is larger than the magnetic volume or volume of magnetic nanoparticles and V_M is stated as:

$$V_H = \frac{\pi(D+2\delta)^3}{6} \text{ and } V_M = \frac{\pi D^3}{6} \quad (29)$$

where, δ is the ligand layer thickness. Since, the actual equilibrium susceptibility χ_o is dependent on the magnetic field assumed to be the chord susceptibility corresponding to the Langevin equation, given by

$$\chi_o = \chi_i \frac{3}{\xi} \left(\coth \xi - \frac{1}{\xi} \right) \quad (30)$$

where, $\chi_i = \frac{\mu_o \phi M_d^2 V_M}{3 k_B T}$, $\xi = \frac{\mu_o M_d H_o V_M}{k_B T}$, $M_s = \phi M_d$, M_d is the domain magnetization of a suspended nanoparticle, and ϕ is the volume fraction of nanoparticles in the ferrofluid, M_d is the bulk saturation magnetization. The magnetic fluid concentration or volume fraction of nanoparticles is calculated as follows:

$$\phi = n \frac{V_M}{V} \quad (31)$$

where, n is the number of magnetic nanoparticles being used, V_M is the magnetic volume of one magnetite particle, and V is the tumour volume. It must be emphasized that greater the volume fraction is than lesser will be critical thermal energy (CTE) requirement by the treatment for achieving same results. However, excessive volume fraction leads to retention of the MNPs in patient's body and is often avoided. Therefore, the best option is to enhance the thermal energy by regulating the AMF characteristics i.e. tune other sensitive parameters like field amplitude, frequency etc. and keeping volume fraction as minimal as possible.

The Relative permeability of ferrofluid with 5% volume fraction ratio of magnetite nanoparticles can be calculated by using Maxwell-Garnette theory

$$\mu_{r,ferrofluid} = \frac{1+2\phi\beta}{1-\phi\beta} \quad (32)$$

where, β is magnetic contrast factor and is calculated as:

$$\beta = \frac{\mu_{r,MNP} - \mu_{r,medium}}{\mu_{r,MNP} + 2\mu_{r,medium}} \quad (33)$$

where, $\mu_{r,ferrofluid}$, $\mu_{r,MNP}$, $\mu_{r,medium}$ are relative permeabilities of ferrofluid, magnetite nanoparticles and medium respectively. The exposure to fields where the product of H.f must not exceed $4.85 \times 10^9 \text{ Am}^{-1}\text{s}^{-1}$ is considered as safe and tolerable as per Atkinson, Brezovich safer exposure condition. Generally, the useable range of frequencies and amplitudes is considered to be $f = 0.05\text{--}1.2 \text{ MHz}$ and $H = 0\text{--}15 \text{ kAm}^{-1}$. Also, the reasonable assumption is that 5-10 mg of magnetic material concentrated in each

cm^3 of tumour tissue is appropriate for magnetic hyperthermia in human patients. While volume fraction can be homogeneous, linear, parabolic distribution as a function of distance from the center of the tumour. Wu et al., 2015 considered a total of 10 mg Fe/g of tumour corresponds to a volume fraction of 0.003. They had used Helmholtz coils and use 5 A ac current in the coils at 300 kHz. While Pavel et al., 2009b mentioned that loss power should be less than $7.5 \times 10^9 \text{ W/m}^3$ values that corresponds to a field amplitude less than 7 kA/m and field frequency less than 250 kHz when considered particles of 18 nm in diameter (with a superparamagnetic behavior) and to a field frequency less than 15 kA/m and respectively 500kHz for particles that describes a hysteric behavior. While Pavel et al., 2008 reported for the superparamagnetic regime, that the optimum loss power for therapy was obtained for magnetite for frequencies between 500 – 550 kHz using a field amplitude H of 6.5 kA/m and particle radius of 9-10 nm. H and f are closely dependent on each other i.e. if one parameter is increased, the other parameter can be decreased and adjusted. Therefore, different field amplitude, frequency and dosage combinations can be adjusted based on tumour dimensions. Considering $H=13.5 \text{ kA/m}$ and frequencies range between 160 and 180 kHz for the maximum biocompatible value of $H=20 \text{ kA/m}$, the frequency must be less than 90 kHz. Zakariapour et al., 2017 used nanoparticles size of 5, 5.5, 6 nm, the strength of the applied alternating current magnetic field ranging from 50, 62, 75 mT with volume fraction ranging from 0.0004, 0.0006, 0.0008 and the frequency of the applied AC magnetic field ranging from 300, 400, 500 kHz results in increasing temperature respectively. Salarian et al., 2011 had discussed the effect of various combinations i.e. $H=10 \text{ kA/m}$, 14 kA/m , 18 kA/m , frequency 300 kHz, 500 kHz, 700 kHz, diameter of nanoparticles 5 nm, 6 nm, 7 nm, different types of nanoparticles, nanoparticle volume fractions 0.0004, 0.0006, 0.0008. Miaskowski and Sawicki, 2013 had reported a coupled study with a mixture model incorporating volume fraction, superparamagnetic heating, with dextran coated magnetite nanoparticle of 19 nm size. They had used 5 turn coil with current $I=400 \text{ A}$ and operating frequency of 150 kHz fulfilling the Atkinson's condition as mentioned in the context of phantom measurements. They had used magnetic fluid concentration as 40×10^{-6} . Hilger et al., 2005a,b for breast cancer considerations had mentioned that the tumour lesions with diameter of 3 mm - 20 mm could be treated using a carefully adjusted magnetite amount. They have used AC magnetic field (frequency of 410 kHz and amplitude 8.8 kA/m). Hilger et al., 2001 had reported 14 kA/m and 300 kHz as frequency. Also they had deduced that a frequency of 400 kHz and an amplitude of 6.5 kA/m may be tolerable for the exposure of the parts of the body with diameters of up to 15 cm if shorter exposure times are used. They had injected 21 mg of magnetite intratumorally. Further, they had reported no frequency based variations in tissue penetrations and also the inhomogeneity of the field amplitude across the animal body region of interest was considered negligible. Further, as per their reported findings, tumours with volumes of approximately 300 mm^3 can be heated and no potential problems with heating larger tissue volumes ($\geq 1000 \text{ mm}^3$): for our study the breast tumour is having a volume of 2572 mm^3 with 1.7 cm in size. Salloum et al., 2008 reported magnetic frequency variations from 63 kHz to 700 kHz while the lower and the upper limits of magnetic field strengths were 3 and 24.8 kA/m. Particle size used are all smaller than

15 nm in diameter. They had used a two-turn water cooled coil of 20 cm in diameter and 7 cm in height to generate a magnetic field inside the coil. They had used radiofrequency generator to induce an alternating current of 384 A at a frequency of 184 kHz. They had used water-based ferrofluid with a concentration of 3.3% by volume and a particle size of 10 nm i.e. within each 0.1 cc of ferrofluid contains 17.3 mg of solid iron oxide. Kumar and Attaluri et al., 2013 used amplitude of AMFs >50 kA/m and frequency of 160 kHz. They had mentioned frequency adjustments in the range of 135 kHz to 440 kHz. Also, Hilger et al., 2005a shows magnetite [10 nm superparamagnetic behavior] (21 mg±9 magnetite per 299 mm³ target tissue used field amplitude of 6.5 kA/m, frequency 400 kHz, treatment time 242 s and maximum temperatures of 71°C). Rast et al., 2010 had reported magnetic field strengths in the range of $0 < H < 15$ kA/m and frequencies $0.05 < f < 1.2$ MHz and had manipulated SAR based on frequency of 300 kHz and field amplitude of 6.5 kA/m by doing extrapolation to SAR which raised from 45 W/g to 209 W/g at 14 kA/m. Hergt et al., 2010 shows superparamagnetic relaxation graphically by plotting particle diameter vs. field amplitude. It can be concluded from the graph that superparamagnetic region lies below 20 nm particle diameter size and field amplitude up to 50 kA/m. Below this size of 20 nm only Neel relaxation contributes towards heating. They have plotted another graph and shows that losses per cycle are maximum with nanoparticle diameter of 19 nm and amplitude of external magnetic field as 30 kA/m.

References

1. Wu L., Cheng J., Liu W., and Chen X., 2015. Numerical Analysis of Electromagnetically Induced Heating and Bioheat Transfer for Magnetic Fluid Hyperthermia. *IEEE Trans. On Magn.*, 51(2):4600204.
2. Pavel M. and Stancu A., 2009b. Ferromagnetic nanoparticles dose based on tumor size in magnetic fluid hyperthermia cancer therapy. *IEEE Trans. on Magn.*; 45(11): 5251-5254.
3. Pavel M., Gradinariu G., and Stancu A., 2008. Study of the optimum dose of ferromagnetic nanoparticles suitable for cancer therapy using MFH. *IEEE Trans. on Magn.*; 44(11): 3205-3208.
4. Salloum M., Ma R., Zhu L., 2008. An In-vivo experimental study of temperature elevations in animal tissue during magnetic nanoparticle hyperthermia. *Int J. Hyperthermia*; 24(7): 589-601.
5. Hilger, I., Andrä, W., Hergt, R., Hiergeist, R., Schubert, H., Kaiser, W.A., 2001. Electromagnetic heating of breast tumours in interventional radiology: in-vitro and in-vivo studies in human cadavers and mice. *Radiology* 218, 570-575.
6. Hilger, I., Hergt, R., Kaiser, W.A., 2005a. Towards breast cancer treatment by magnetic heating. *J. Magn. Magn. Mater.* 293, 314-319.
7. Hilger, I., Hergt, R., Kaiser, W.A., 2005b. Use of magnetic nanoparticle heating in the treatment of breast cancer. *IEEE Proc. on Nanobiotechnol.* 152, 33-39.
8. Miaskowski, A., Sawicki, B., 2013. Magnetic fluid hyperthermia modelling based on phantom measurements and realistic breast model. *IEEE Trans. on Biomed. Eng.* 60, 1806-1813.

9. Zakariapour, M., Hamed, M.H., Fatourae, N., 2017. A numerical study of magnetic nanoparticles hyperthermia with alternating magnetic field under influence of convection heat transfer. *J. Eng. Sci. Tech.* 12, 405-422.
10. Salarian H., Garmabaki H.S., Zakariapour M., Ghorbani B., Amidpour M., 2011. A Numerical Study of heating effect of magnetic nanoparticles Hyperthermia with alternating magnetic field. *Proc. of Int. Conf. on Advances in Mechanical Engineering*, 11-15.
11. Pavel M. and Stancu A., 2009b. Ferromagnetic nanoparticles dose based on tumor size in magnetic fluid hyperthermia cancer therapy. *IEEE Trans. on Magn.*; 45(11): 5251-5254.
12. Kumar A., Attaluri A., Mallipudi R., Cornejo C., Bordelon D., Armour M., Morua K., DeWeese T.L., and Ivkov R., 2013. Method to reduce non-specific tissue heating of small animals in solenoid coils. *Int J. Hyperthermia*, 29(2): 106-120.
13. Rast L. and Harrison J.G., 2010. Computational Modeling of Electromagnetically Induced Heating of Magnetic Nanoparticle Materials for Hyperthermic Cancer Treatment. *PIERS Online*, 6: 690-694.
14. Hergt R., Dutz S., and Zeisberger M, 2010. Validity limits of the Neel Relaxation model of magnetic nanoparticles for hyperthermia. *Nanotechnology*, 21:015706 (1-5).